# Self-Organization of Rod−Coil Molecules with Layered Crystalline States into Thermotropic Liquid Crystalline Assemblies

**Myongsoo Lee,*,† Byoung-Ki Cho,† Heesub Kim,‡ Ju-Young Yoon,‡ and Wang-Cheol Zin‡**

*Contribution from the Department of Chemistry, Yonsei University, Shinchon 134, Seoul 120-749, Korea, and Department of Materials Science and Engineering, Pohang University of Science and Technology, Pohang 790-784, Korea*

*Received February 27, 1998*

**Abstract:** The synthesis and characterization of the rod−coil molecules of ethyl 4-[4-[oxypoly(propyleneoxy)-propyloxy]-4′-biphenylcarboxyloxy]-4′-biphenylcarboxylate with poly(propylene oxide) coil of 7 (**7-P-4**), 8 (**8-P-4**), 10 (**10-P-4**), 12 (**12-P-4**), 15 (**15-P-4**), 17 (**17-P-4**), and 20 (**20-P-4**) propylene oxide units are described. The introduction of poly(propylene oxide) (PPO) coils with different lengths into the rodlike mesogen gives rise to a rich self-assembled microstructures. In the crystalline state, the rod−coil molecules with 7−12 repeating units of PPO organize into a microphase-separated monolayer lamellar structure in which rods are fully interdigitated. In contrast, the rod−coil molecules with 15−17 repeating units of PPO exhibit a lamellar structure with rod tilt relative to the layer normal. A dramatic mesophase change is observed with the variation of the coil length. The rod−coil molecules **7-P-4** and **8-P-4** with short PPO coils display layered smectic C and smectic A mesophases, while the rod−coil molecules **10-P-4**, **12-P-4**, and **15-P-4** with medium-length coils exhibit a biconticuous cubic mesophase with *Ia*3*d* symmetry. Further increasing the length of coils as in the cases of **15-P-4**, **17-P-4**, and **20-P-4** induces a hexagonal columnar mesophase. Estimations based on the lattice parameters and densities have shown that the organization of the rod−coil molecules into a cross sectional slice of a cylinder for the cubic and columnar phases can give rise to an aromatic core with a square cross section. This unique behavior in the rod−coil molecules is believed to originate from the anisotropic aggregation of rod segments and consequent entropic penalties associated with coil stretching.

## Introduction

Rodlike molecules have been widely studied and found to exhibit thermotropic liquid crystalline ordered phases such as nematic and/or layered smectic types of supramolecular structures in which the molecules are arranged with their long axes parallel to each other. For these molecules, the main factor governing the geometry of supramolecular structure in the liquid crystalline phase is anisotropic aggregation of the molecules.[1] In contrast, coil−coil diblock molecules consisting of different immiscible coil segments have been found to exhibit a wide range of microphase-separated supramolecular structures with curved interfaces in addition to layer structures.[2] This phase behavior is understood to be mainly due to the mutual repulsion of the dissimilar blocks and the packing constraints imposed by the connectivity of each block.[3]

Rod−coil molecules consisting of a rigid rod block and a flexible coil block can provide a novel class of self-assembling materials since the molecule shares certain general characteristics of both diblock molecules and thermotropic calamitic molecules. The driving forces controlling the phase behavior of rod−coil molecules are expected to be quite different from those of conventional flexible block copolymers or rodlike molecules due to the presence of microphase separation of the coil and rod blocks into ordered periodic structures as well as the tendency of the rod block to form anisotropic orientationally ordered structures.

In comparison to the extensive works on both coil−coil diblock copolymers and liquid crystalline rodlike molecules, only a few works on the phase behavior of rod−coil system have been performed.[4−8] In contrast to coil−coil diblock molecules, rod−coils have substantial packing problems in the microphase-separated state. At the interface separating the rod and coil domains, the relatively smaller area per junction favored by the rod block results in chain stretching of the coil block, which is energetically unfavorable. Considering the energetical penalties associated with chain stretching of the coil block and interfacial energy resulting from the interfaces separating the rod and coil domains, the theoretical works on rod−coil systems have predicted nematic−smectic A and smectic A−smectic C

* To whom all correspondence should be addressed. Fax: 82-2-364-7050. E-mail: mslee@alchemy.yonsei.ac.kr.

† Yonsei University.

‡ Pohang University of Science and Technology.

(1) Stegemeyer, H., Ed. *Liquid Crystals*; Springer: New York, 1994.

(2) (a) Bates, F. S.; Fredrickson, G. H. *Annu. Rev. Phys. Chem.* **1990**, *41*, 525. (b) Hasegawa, H.; Tanaka, H.; Yamasaki, K.; Hashimoto, T. *Macromolecules* **1987**, *20*, 1651. (c) Hashimoto, T.; Shibayama, M.; Kawai, H. *Macromolecules* **1983**, *16*, 1093.

(3) (a) Helfand, E.; Wasserman, Z. R. *Macromolecules* **1980**, *13*, 994. (b) Leibler, L. *Macromolecules* **1980**, *13*, 1602. (c) Ohta, T.; Kawasaki, K. *Macromolecules* **1986**, *19*, 2621.

(4) (a) Semenov, A. N.; Vasilenko, S. V. *Sov. Phys.-JEPT (Engl. Transl.)* **1986**, *63*, 70. (b) Semenov, A. N. *Mol. Cryst. Liq. Cryst.* **1991**, *209*, 191.

(5) (a) Halperin, A. *Macromolecules* **1990**, *23*, 2724. (b) Petschek, R. G.; Wiefling, K. M. *Phys. Rev. Lett.* **1987**, *59*, 343.

(6) (a) Raphael, E.; de Genn, P. G. *Makromol. Chem., Macromol. Symp.* **1992**, *62*, 1. (b) Raphael, E. *Physica A* **1991**, *177*, 294.

(7) (a) Radzilowski, L. H.; Stupp, S. I. *Macromolecules* **1994**, *27*, 7747. (b) Radzilowski, L. H.; Carragher, B. O.; Stupp, S. I. *Macromolecules* **1997**, *30*, 2110. (c) Stupp, S. I.; LeBonheur, V.; Walker, K.; Li, L. S.; Huggins, K. E.; Keser, M.; Amstutz, A. *Science* **1997**, *276*, 384.

(8) (a) Chen, J. T.; Thomas, E. L.; Ober, C. K.; Hwang, S. S. *Macromolecules* **1995**, *28*, 1688. (b) Chen, J. T.; Thomas, E. L.; Ober, C. K.; Mao, G. *Science* **1996**, *273*, 343.

S0002-7863(98)00654-4 CCC: $15.00 
Published on Web 08/28/1998

transitions in the melt.[4] Other theoretical works have dealt more with the phase behavior of rod−coil diblocks in a selective solvent for the coil segment.[5] These works have predicted various micellar structures for sufficiently large coil volume fraction, in addition to the familiar lamellar structures. Theoretical treatments of flexible−rigid−flexible triblock copolymers have also predicted fence and needlelike morphologies.[6]

Experimentally, rod−coil molecules consisting of a rod block and a flexible coil block are reported to show lamellar or micellar microphase-separated domains depending on the volume fraction of coil segments in the molecules, although molecular order within the rod blocks in the melt state was not described.[7,8] Recently our works have shown that the rod−coil molecules consisting of a molecular rod and a poly(ethylene oxide) coil exhibit a microphase-separated lamellar structure in the crystalline phase as well as in the melt state, leading to a smectic type of supramolecular structure.[9] The binary mixture of these rod−coil molecules and lithium triflate has been shown to induce cubic and cylindrical micellar mesophases, depending on the salt concentrations.[9,10] The results suggest that varying the salt concentration in rod−coil molecule is analogous to changing the solvent content in lyotropic amphiphilic system or varying the volume fraction of each block in coil−coil diblock copolymers. However, the equilibrium supramolecular structures of rod−coil molecules and their formation mechanism are expected to be significantly different from those of coil−coil diblock systems due to the distinctive properties of rodlike blocks. Thus apparent elucidation of the unique phase behavior on rod−coils requires the synthesis and characterization of the rod−coil molecules with systematic variation of the coil length.

The design of rod−coil diblock molecules described here was based on that of an extended rodlike molecule consisting of two biphenyl units.[11] The extended rods of this type can exhibit calamitic mesomorphism; however, unlike coil−coil diblock macromolecules, rod molecules cannot be easily arranged into cubic or columnar phases due to steric reasons associated with their oblate shape. To introduce block segregation character, we synthesized rod−coil diblock molecules consisting of a molecular rod and a poly(propylene oxide) coil which is not prone to crystallize due to the side methyl group in propylene oxide unit. This article reports the synthesis of rod−coil molecules containing poly(propylene oxide) (PPO) as a flexible coil (***n*-P-4**, where *n* represents the number of repeating units of PPO coil) and their phase behavior characterized by optical polarized microscopy, differential scanning calorimetry (DSC), and X-ray diffraction measurements. A rich variety of supramolecular architectures will be also demonstrated to be induced in a molecular rod system through introduction of a flexible coil with different lengths.

## Results and Discussion

**Synthesis.** The synthesis of rod−coil molecules containing poly(propylene oxide)s with various degrees of polymerization was performed through the similar procedure described previously.[11] Commercially available poly(propylene oxide)s with degrees of polymerization of 7, 12, and 17 and synthesized poly(propylene oxide)s with degrees of polymerization of 8, 10, 15, and 20 were used as starting materials for rod−coil molecules

**Scheme 1**. Synthesis of Rod−Coil Molecules ***n*-P-4**

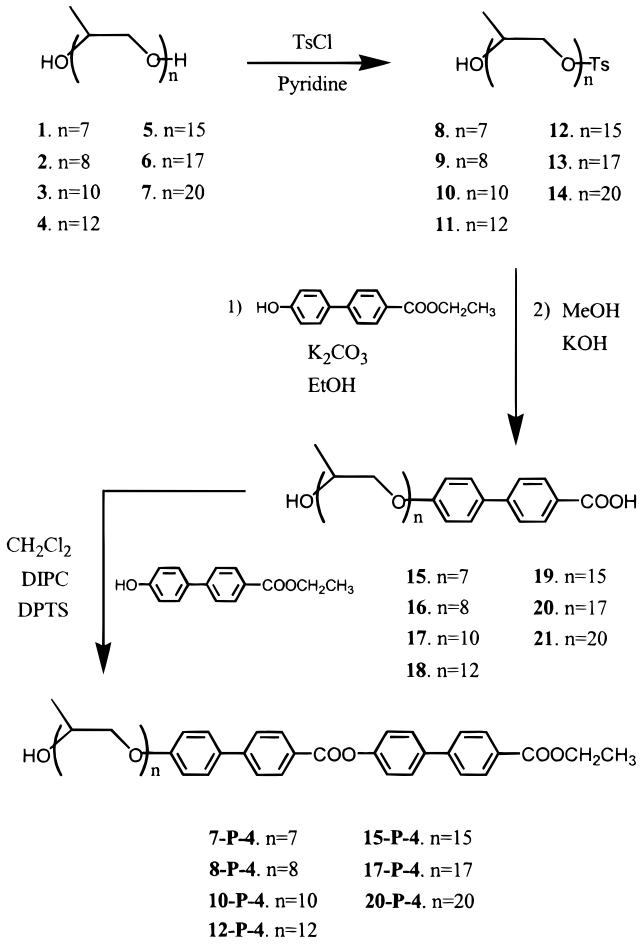


as outlined in Scheme 1. The appropriate poly(propylene oxide) reacted with *p*-toluenesulfonyl chloride to yield monotosylated poly(propylene oxide). Substitution reaction of monotosylated poly(propylene oxide) with ethyl 4-hydroxy-4′-biphenylcarboxylate produced an intermediate which was further hydrolyzed to yield compounds **15**−**21**. The rod−coil molecules (***n*-P-4**) were obtained by treating (25 °C, 12 h) **15**−**21** with ethyl 4-hydroxy-4′-biphenylcarboxylate in $CH_2Cl_2$ in the presence of diisopropylcarbdiimide (DIPC) and 4-(dimethylamino)pyridinium−*p*-toluene sulfonate (DPTS). The resulting rod−coil molecules were purified by column chromatography (silica gel) using ethyl acetate as an eluent until transition temperatures remained constant.

It is well-known that polydispersity influences the phase behavior of the polymers, especially those with low molecular weight.[12] Therefore, it is essential that the rod−coil molecule is highly monodisperse to investigate its accurate phase behavior. Table 1 shows the characterization of the rod−coil molecules. All of the rod−coil molecules showed a monomodal molecular weight distribution less than 1.1 of the polydispersity determined from GPC indicative of high purity. The chemical structure of the rod−coil molecules and the number of repeating units in poly(propylene oxide) were confirmed by $^1$H NMR spectroscopy. The number of repeating units in the poly(propylene oxide) coil of rod−coil molecules determined from the ratio of the aromatic protons (ortho to alkoxy) to the ethylene protons of poly(propylene oxide) was in good agreement with the expected value.

(9) (a) Lee, M.; Oh, N.-K. *J. Mater. Chem.* **1996**, *6*, 1079. (b) Lee, M.; Oh, N.-K.; Lee, H. K.; Zin, W.-C. *Macromolecules* **1996**, *29*, 5567.

(10) (a) Lee, M.; Oh, N.-K. *Mol. Cryst. Liq. Cryst.* **1996**, *280*, 283. (b) Lee, M.; Zin, W.-C.; Ji, S. W. *Bull. Kor. Chem. Soc.* **1996**, *17*, 309.

(11) (a) Lee, M.; Oh, N.-K.; Zin, W.-C. *Chem. Commun.* **1996**, 1787. (b) Lee, M.; Cho, B.-K.; Kim, H.; Zin, W.-C. *Angew. Chem., Int. Ed.* **1998**, *37*, 638.

(12) Percec, V.; Lee, M. *Macromolecules* **1992,** *24*, 2780.

**Table 1.** Characterization and Thermal Transitions of Diblock Rod−Coil Molecules[a,b]

| rod−coil molecule | DP[c] of coil | $M_w/M_n$[d] | phase transitions (°C) and corresponding enthalpy changes (kJ/mol) | |
|---|---|---|---|---|
| | | | heating | cooling |
| **7-P-4** | 7.2 | 1.04 | k 61.0 (19.5) $s_C$ 107.5 (0.2) $s_A$ 122.4 (0.9)i<br>k 47.8 (1.8) k 62.1 (9.8) $s_C$ 108.6 (0.2) $s_A$ 122.8 (0.9) i | i 120.4 (1.1) $s_A$ 106.2 (0.2) $s_C$ 53.7 (1.1) k 44.2 (3.7) k |
| **8-P-4** | 8.1 | 1.04 | k 56.7 (20.1) $s_C$ 97.0 (0.3) $s_A$ 103.3 (0.2) i<br>k 43.4 (5.1) k 57.6 (11.8) $s_C$ 97.2 (0.2) $s_A$ 102.7 (0.3) i | i 101.1 (0.3) $s_A$ 95.0 (0.2) $s_C$ 48.0 (1.0) k 39.1 (3.7) k |
| **10-P-4** | 10.2 | 1.04 | k 51.8 (20.5) cub 87.6 (1.7) i<br>k 52.7 (21.7) cub 88.0 (1.4) i | i 72.7 (1.0) cub 9.2 (2.7) k |
| **12-P-4** | 11.9 | 1.08 | k 36.9 (17.6) cub 68.1 (1.0) i<br>k 38.7 (10.4) cub 69.6 (1.2) i | i 61.6 (1.1) cub 4.9 (0.1) k |
| **15-P-4** | 14.9 | 1.05 | k 19.9 (4.4) cub 41.2 (0.4) col 46.2 (0.5) i<br>k 23.0 (11.9) cub 41.1 (0.5) col 46.1 (0.5) i | i 43.5 (0.5) col 36.3 (0.5) cub 11.1 (0.3) k |
| **17-P-4** | 17.0 | 1.05 | k 20.1 (2.5) col 46.2 (0.7) i<br>k 22.0 (4.1) col 46.5 (0.5) i | i 39.8 (0.5) col 19.0 (1.9) k |
| **20-P-4** | 20.0 | 1.04 | k 19.4 (2.3) col 41.0 (0.6) i<br>k 19.2 (2.1) col 41.4 (0.8) i | i 36.2 (0.7) col 17.2 (2.1) k |

[a] Data on the first line are from first heating and cooling scans; data on second line are from second heating scan. [b] k = crystalline, $s_C$ = smectic C, $s_A$ = smectic A, cub = cubic, col = hexagonal columnar, i - isotropic. [c] Determined from NMR data. [d] Determined from GPC data.

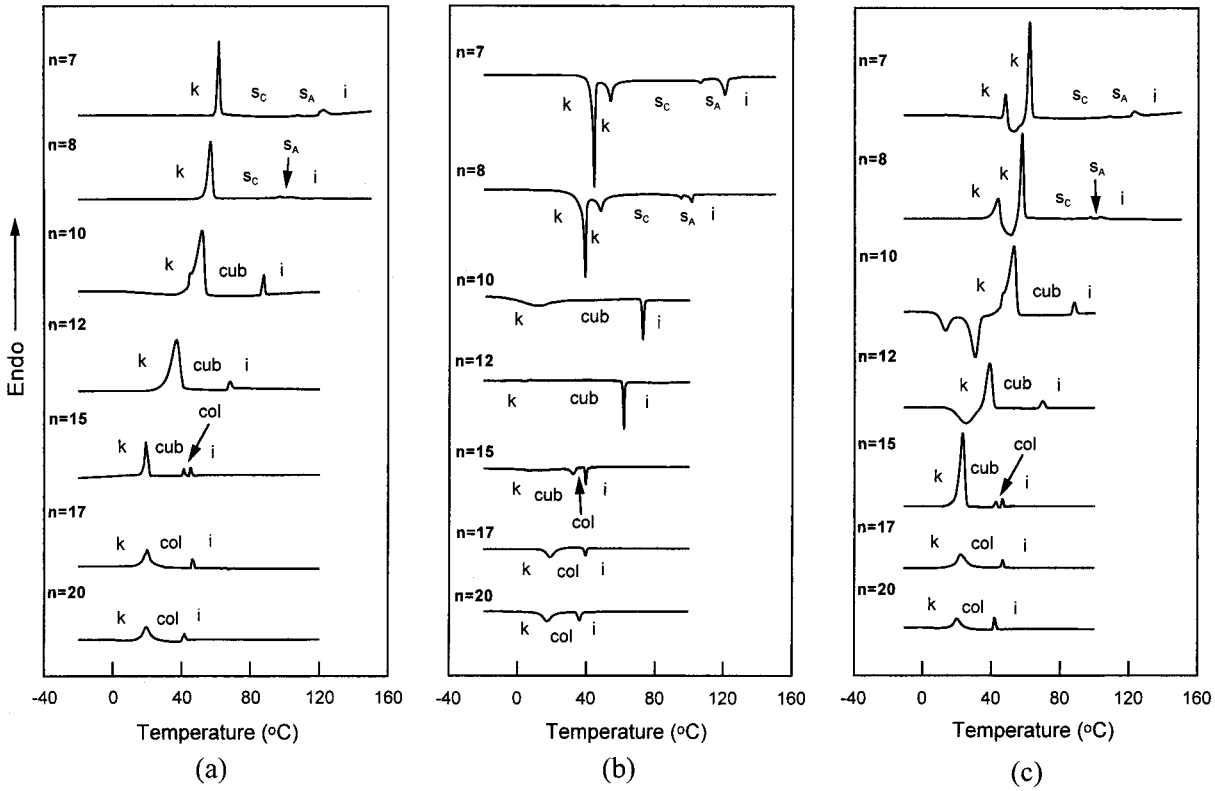


**Figure 1.** DSC traces exhibited during (a) the first heating scan, (b) the first cooling scan, and (c) the second heating scan by ***n*-P-4** with different numbers of repeating units (*n*) of poly(propylene oxide) coil.

**Thermotropic Phase Behavior.** The phase behaviors of the resulting rod−coil molecules were characterized by a combination of techniques consisting of differential scanning calorimetry (DSC), thermal optical polarized microscopy, and X-ray scattering experiments. Figure 1 presents the DSC first heating, the first cooling, and the second heating traces of the rod−coil molecules. The DSC traces obtained during the second and subsequent heating scans are almost identical. The transition temperatures and the corresponding enthalpy changes of all the rod−coil molecules obtained from DSC heating and cooling scans are summarized in Table 1. As can be observed from Figure 1, rod−coil molecule **7-P-4** exhibits a crystalline phase which melts and recrystallizes into a second crystal phase, followed by a smectic C phase which, in turn, undergoes transformation into a smectic A phase on second heating. Optical microscopic observations of this compound are consistent with this behavior. Transition from an isotropic liquid can be seen by the rapid formation of batonnets which merge into a focal conic fanlike texture with pseudoisotropic areas indicating a smectic A phase.[13] On further cooling, a transition to a schlieren texture which is consistent with a smectic C mesophase can be observed.[13] Rod−coil molecule **8-P-4** shows a phase behavior similar to that of **7-P-4** with the exception of a lower transition temperature.

In marked contrast, no birefringence between crossed polarizers after melting could be observed for rod−coil molecules **10-P-4** and **12-P-4**. In addition to a crystal melting transition, DSC results indicate an additional phase transition at higher

(13) (a) Demus, D.; Richter, L. *Textures of Liquid Crystals*; Verlag Chemie: Weinheim, Germany, 1978. (b) Gray, G. W.; Goodby, J. W. *Smectic Liquid Crystals. Textures and Structures*; Leonard Hill: Glasgow, U.K., 1984.

**Table 2.** Characterization of the Rod-Coil Molecules by Small-Angle X-ray Scattering

| rod−coil molecule | density $\rho$ (g/mL) | | crystalline phase | | smectic phase | | cubic phase | | | columnar phase | | |
|---|---|---|---|---|---|---|---|---|---|---|---|---|
| | 10 °C | 25 °C | calcd length[a] (Å) | $d_{001}$ (Å) | $d_{001}$ ($s_C$) (Å) | $d_{001}$ ($s_A$) (Å) | $d_{211}$ (Å) | lattice constant ($a$) (Å) | $n$ | $d_{100}$ (Å) | lattice constant ($a$) (Å) | $n$ |
| **7-P-4** | 1.14 | | 52.9 | 55.0 | 43.3 | 45.9 | | | | | | |
| **10-P-4** | 1.11 | | 65.3 | 64.2 | | | 44.9 | 110 | 4.7 | | | |
| **12-P-4** | 1.10 | | 73.6 | 76.5 | | | 49.4 | 121 | 5.1 | | | |
| **15-P-4** | 1.08 | 1.05 | 86.1 | 74.6 | | | 53.9 | 132 | 5.2 | 49.8 | 57.5 | 7.3 |
| **17-P-4** | 1.07 | 1.04 | 94.4 | 77.1 | | | | | | 52.5 | 60.6 | 7.3 |
| **20-P-4** | 1.07 | 1.04 | 106.8 | | | | | | | 55.0 | 63.5 | 7.2 |

[a] Calculated lengths of the rod−coil molecules are based on density measurements. $n$ = number of molecules per column cross section.

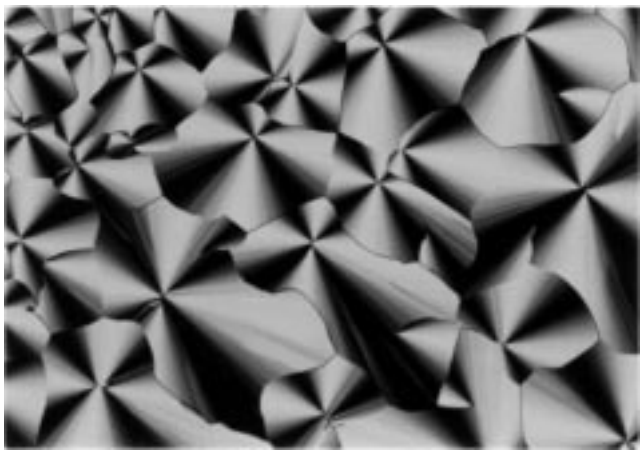

**Figure 2.** Representative optical polarized micrograph (100×) of the texture exhibited by the hexagonal columnar mesophase of **20-P-4** at 35 °C on a cooling scan.

temperature which is accompanied by a sudden significant decrease of viscosity, strongly suggesting the existence of a cubic mesophase.[13,14] On shearing birefringence of a mosaic texture could be observed, which persists for a few seconds. In a stress-free state, the mosaic texture disappears gradually to recover an optically isotropic state.

Rod−coil molecule **15-P-4** exhibits a crystalline melting transition into an optical isotropic cubic mesophase, followed at higher temperatures by a hexagonal columnar mesophase which, in turn, undergoes isotropization at 46.0 °C. On cooling from the isotropic liquid, first a spherulitic growing of texture can be observed with a final development of pseudo-focal conic domains which are characteristic of a hexagonal columnar mesophase exhibited by conventional discotic mesogens.[15] On further cooling from the hexagonal columnar phase, isotropic rectangular and rhombic areas with straight edges appear and these regions then grow until the entire field of view is dark, which is characteristic of the cubic mesophase.[14] In the rod−coil molecules with higher degrees of polymerization (DPs) of poly(propylene oxide) coil, the cubic phase disappears as in the case of rod−coil molecules **17-P-4** and **20-P-4**. They display only an enantiotropic hexagonal columnar phase after crystalline melting. A representative texture exhibited by a hexagonal columnar mesophase of **20-P-4** is shown in Figure 2.

The thermal behavior of the rod−coil molecules determined from the second heating and the first cooling DSC scans as well as thermal optical polarized microscopy is presented in Figure 3. As shown in Figure 3, the transition temperatures associated with the mesomorphic−isotropic phase decrease and crystallization is suppressed with increasing the number of repeating units of poly(propylene oxide) coil. The ability of the rod−coil molecules to form liquid crystalline phases is not inhibited by the presence of the flexible poly(propylene oxide) coil block, even for **20-P-4**, which contains 76% coil by weight. The microphase separation between rod and coil blocks in addition to the anisotropic nature of the rod block seems to play a major role in the self-assembly of the rod−coil molecules. A unique feature observed in Figure 3 consists of the differences in the degree of supercooling associated with crystallizations at each mesophase (Figure 3a vs Figure 3b). The degree of supercooling at the cubic−crystalline transition is much higher compared to those of both smectic−crystalline and columnar−crystalline transitions, which represents a strong kinetic effect. This indicates that considerable structural change may occur at the transition from cubic to crystalline phases.[16] Considering that the crystalline structure is a lamellar, which will be discussed later, this transition, indeed, corresponds to the change from three-dimensional (cubic) to one-dimensional (lamellar) geometry.

**Characterization of Microstructures by X-ray Diffraction.** To investigate the microstructures of the crystalline solid and liquid crystalline phases, X-ray scattering experiments have been performed with the rod−coil molecules at various temperatures. The X-ray diffraction patterns of all the rod−coil molecules in the crystalline state display three reflections with the ratio of reflection positions of 1:2:3 in the small-angle region, while two sharp reflections are observed in the wide-angle region, indicative of a lamellar structure consisting of a microphase-separated crystalline rod domains and the amorphous poly(propylene oxide) coil domains. The layer spacings measured at the crystalline phase for all the rod−coil molecules are summarized in Table 2, together with the corresponding molecular lengths estimated from density measurements. The layer spacings are very close to the corresponding estimated molecular lengths for the rod−coil molecules with 7−12 repeating units of poly(propylene oxide) coil, indicative of a monolayer lamellar structure in which rods are fully interdigitated. In contrast, the layer spacings are smaller than the estimated molecular lengths for the rod−coil molecules containing the coil with 15−17 repeating units, indicating that the rod−coil molecules with higher DPs of poly(propylene oxide) coil organize into a monolayer lamellar structure with rod tilt with respect to the interface separating the rod and coil domains. This packing arrangement of rods is similar to that in a smectic C liquid crystalline phase.

Figure 4 shows the dependence of $d$ spacing of the lamellar structure as a function of the number of repeating units in a poly(propylene oxide) grafted in a rod. The $d$ spacing systematically increases with the DP of poly(propylene oxide) up to 12 and thereafter remains relatively constant. This plot suggests that the extent of the rod tilt increases with increasing the length

(14) Stauffer, G.; Schellhorn, M.; Lattermann, G. *Liq. Cryst.* **1995**, *18*, 519.

(15) Destrade, C.; Foucher, P.; Gasparoux, H.; Nguyen, H. T. *Mol. Cryst. Liq. Cryst.* **1984**, *106*, 121.

(16) Forster, S.; Khandpur, A. K.; Zhao, J.; Bates, F. S.; Hamley, I. W.; Ryan, A. J.; Bras, W. *Macromolecules* **1994**, *27*, 6922.

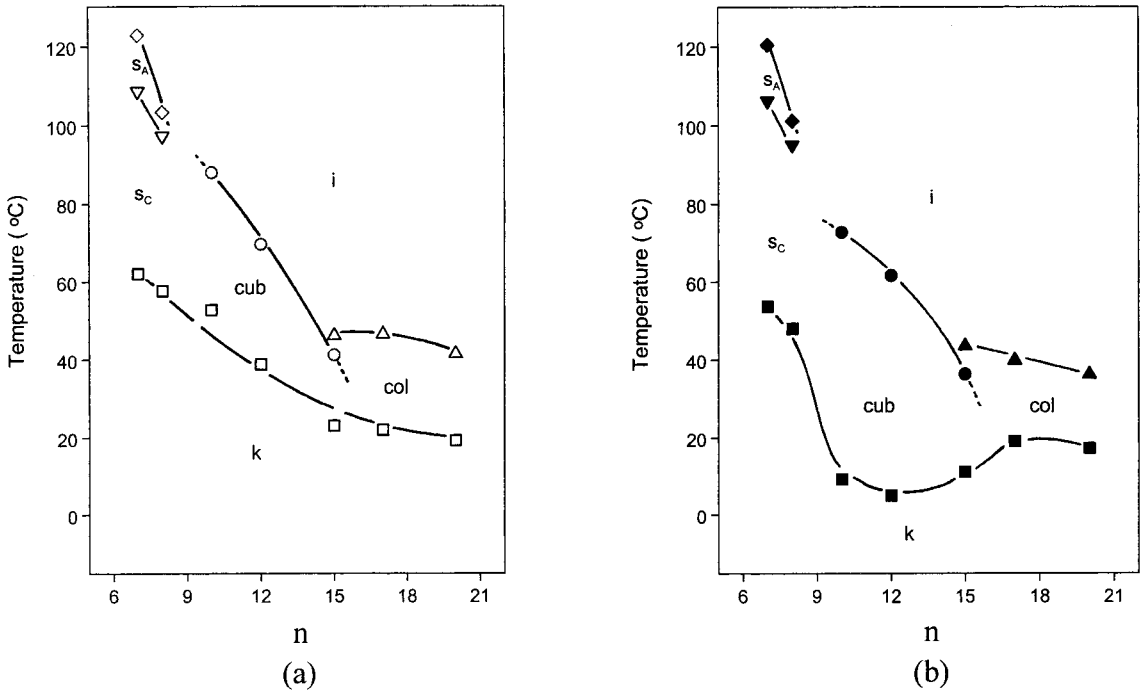


**Figure 3.** Dependence of the transition temperatures of the rod−coil molecules on the number of repeating units ($n$) of poly(propylene oxide) coil. (a) Data from the second heating scan: □, $T_m$; ▽, $T_{s_C-s_A}$; ◇, $T_{s_A-i}$; ○, $T_{cub-i}$; △, $T_{col-i}$. (b) Data from the first cooling scan: ■, $T_m$; ▼, $T_{s_C-s_A}$; ◆, $T_{s_A-i}$; ●, $T_{cub-i}$; ▲, $T_{col-i}$.

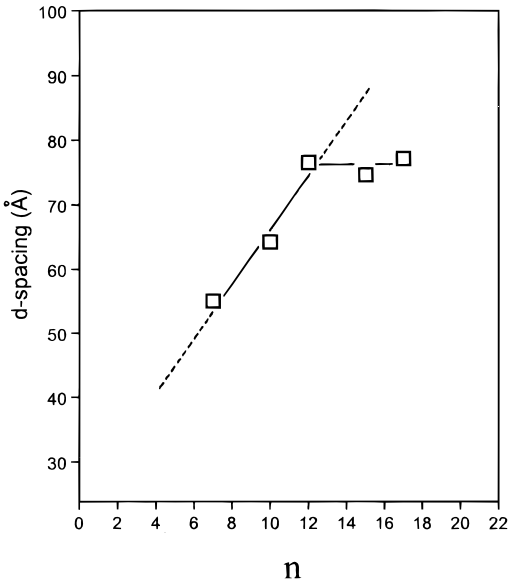


**Figure 4.** Dependence of the $d$ spacing of ***n*-P-4** in the crystalline phase of the rod−coil molecules on the number of repeating units ($n$) of poly(propylene oxide) coil.

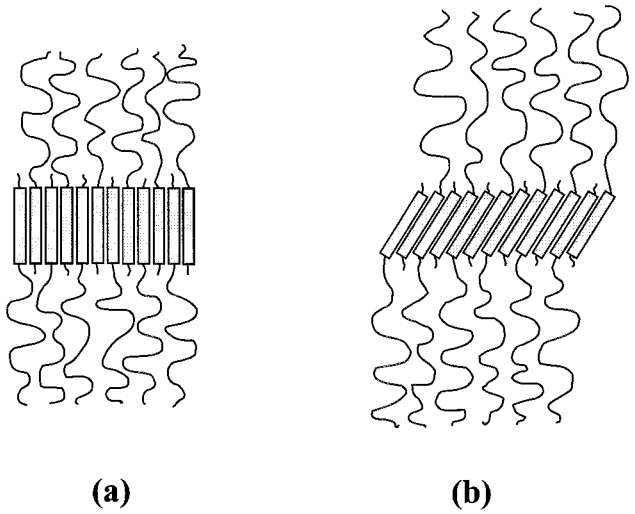


**Figure 5.** Schematic representation of (a) the crystalline lamellar structure of **7-P-4**, **10-P-4**, and **12-P-4** in which rods are fully interdigitated and (b) the crystalline lamellar structure of **15-P-4** and **17-P-4** with rod tilt relative to the layer normal.

of coil at the rod−coil molecules with a higher DP of coil. This is most probably due to the energetic penalties associated with chain stretching of the poly(propylene oxide) coil blocks. The rod tilt has been well illustrated by theories to cause the rod−coil junctions to spread apart, the area per coil increases, and thus, coil stretching penalties are lowered.[4−6] A similar behavior has also been recently observed in the rod−coil polymers based on poly(hexyl isocyanate).[8] Figure 5 shows the schematic representations of possible packing arrangements of rods in the lamellar structure exhibited by the crystalline phase of the rod−coil molecules.

To confirm the mesophase assignments determined from optical microscopic observations, both small-angle and wide-angle X-ray scattering experiments have been performed with the rod−coil molecules at elevated temperatures (Table 2). In the liquid crystalline phase at 130 °C, **7-P-4** exhibits a sharp reflection corresponding to layer spacing of 45.9 Å, indicating that **7-P-4** exhibits a smectic A phase with an interlayer spacing of 45.9 Å periodicity. On cooling to 90 °C, $d$ spacing decreases to 43.3 Å, which corresponds to a tilt angle of 17.0° relative to the layer normal. This result together with optical microscopic observations demonstrates that it exhibits a smectic C mesophase as its intermediate phase.

In the optically isotropic cubic mesophase of **10-P-4, 12-P-4**, and **15-P-4**, a considerable number of sharp reflections in the small-angle region are observed for all the rod−coil molecules. The observed $d$ spacings for each rod−coil molecule are given in Table 2, and a representative small-angle X-ray diffraction pattern of **12-P-4** is shown in Figure 6. As can be

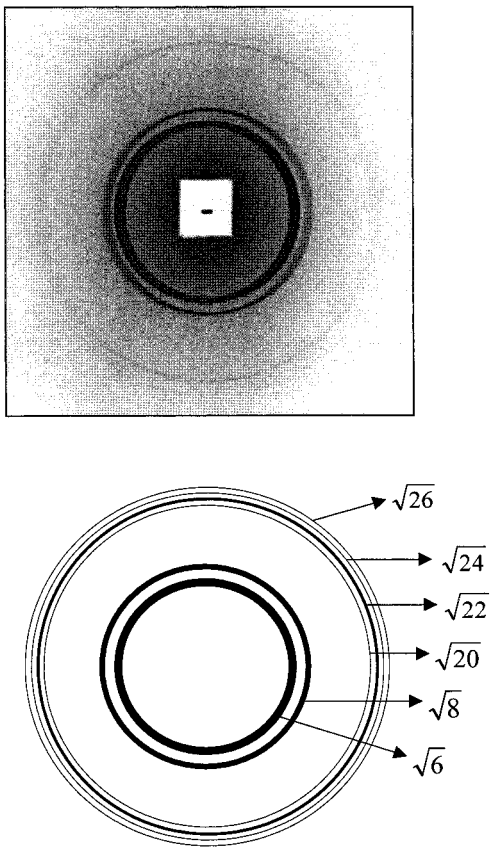


**Figure 6.** Small-angle X-ray diffraction pattern of **12-P-4** in the cubic mesophase at 50 °C.

seen in Figure 6, the sharp reflections are observed at the relative positions of $\sqrt{6}$, $\sqrt{8}$, $\sqrt{20}$, $\sqrt{22}$, $\sqrt{24}$, and $\sqrt{26}$. The positions of these reflections can be indexed as the 211, 220, 420, 332, 442, and 431 reflections of *Ia*3*d* symmetry.[17] From the observed *d* spacing of 211 reflection, the best fit values for the cubic lattice parameters for the cubic phases of **10-P-4**, **12-P-4**, and **15-P-4** are 110, 121, and 132 Å, respectively. At a wide angle only a diffuse halo remains for all of the rod−coil molecules as evidence of the lack of any positional long-range order other than the three-dimensional cubic packing.

On the basis of the X-ray diffraction data described above and the thermal behavior exhibiting as an intermediate phase between the lamellar and columnar structures, the cubic phase can be best described as a bicontinuous cubic phase with *Ia*3*d* symmetry occurring frequently in lyotropic systems.[18] Thus a similar model proposed for the lyotropic bicontinuous cubic phase may be used for its description.[18,19] Assuming that a bicontinuous cubic unit cell with *Ia*3*d* symmetry consists of interwoven networks of branched cylinders, coils are in the outer part of the aromatic core in a cylinder in which the rods are aligned axially with their preferred direction. From the measured cubic lattice constants ($a$) and the densities ($\rho$) (Table 2), the average number ($n$) of molecules per cross sectional area of a cylinder with a thickness ($h$) of 5.35 Å (estimated from the density of the rod blocks and the calculated length of a rod of 20 Å) can be calculated according to eq 1, where $M$ is the

$$n = \frac{a^2 h N_A \rho}{6\sqrt{2}M} \quad (1)$$

molecular mass and $N_A$ is Avogadro's number. **10-P-4**, **12-P-4**, and **15-P-4** are calculated to have approximately five molecules per cross section of a cylinder as shown in Table 2. From the estimated value of the inter-rod distance of 5.35 Å and the calculated length of a rod of 20 Å, the aggregation of five rod−coil molecules in a cross section can be estimated to give rise to a nearly square cross sectional aromatic core 27 Å in width and 20 Å in length, considering that the rods are aligned axially with their preferred direction.[5,6] The unique feature associated with this estimation is the induction of a square cross sectional aromatic core resulting from the organization of rodlike molecules.

Although a bicontinuous cubic phase with *Ia*3*d* symmetry is commonly observed in both lyotropic amphiphilic systems and conventional diblock copolymers, it is rare in thermotropic liquid crystalline system and has been observed only a few systems such as amphiphilic glucitol derivatives,[20] polycatenar silver complexes,[21] and glycolipid derivatives.[22] Thus the induction of a bicontinuous cubic phase from a molecular rod with a flexible chain is unusual taking into account its molecular architecture.

The X-ray diffraction pattern of the birefringent mesophases of **15-P-4**, **17-P-4**, and **20-P-4** displays two sharp reflections with the ratio of $1:\sqrt{3}$ in the small-angle region, characteristic of the two-dimensional hexagonal structure (hexagonally packed array of cylindrical micelles).[15] While only a diffuse halo can be observed in the WAXS pattern, indicating that there are only weak liquid-like arrangements of the rods within the cylinder. These results together with optical microscopic observations support that **15-P-4**, **17-P-4**, and **20-P-4** display a disordered hexagonal columnar mesophase with the lattice constant of 57.5, 60.6, and 63.5 Å, respectively. The observed *d* spacings for each rod−coil molecule are given in Table 2 and a representative small-angle X-ray diffraction pattern of **20-P-4** is shown in Figure 7.

Figure 8 shows the dependence of the cross sectional area of a cylinder ($S$) as a function of the molar volume ($V_m$) of the rod−coil molecules. As expected, the cross sectional area increases with the molar volume of the rod−coil molecule. The extrapolation of this plot gives the base point where $S$ and $V_m$ equal to zero, which is reasonable. To describe the detailed supramolecular structure of the columnar phase, it is useful to calculate the number of molecules per cross sectional slice of a column. From the experimental values of the intercolumnar distance ($a$) and the densities ($\rho$) (Table 2), the average number ($n$) of molecules arranged side by side in a single slice of the cylinders with a thickness ($h$) of 5.35 Å (as discussed above) can be calculated according to eq 2, where $M$ is the molecular

$$n = (\sqrt{3}/2)a^2 h(N_A/M)\rho \quad (2)$$

(17) (a) Luzzati, V.; Spegt, P. A. *Nature* **1967**, *215*, 701. (b) Rancon, Y.; Charvolin, J. *J. Phys. Chem.* **1988**, *92*, 2646. (c) Clerc, M.; Levelut, A. M.; Sadoc, J. F. *J. Phys. II (France)* **1991**, *1*, 1263. (d) Sakurai, S.; Irie, H.; Umeda, H.; Nomura, S.; Lee, H.; Kim, J. K. *Macromolecules* **1998**, *31*, 336.

(18) (a) Mitchell, D. J.; Tiddy, G.; Waring, L.; Bostock, T.; McDonald, M. P. *J. Chem. Soc., Faraday Trans. 1* **1983**, *79*, 975. (b) Charvolin, J. *J. Chim. Phys. Phys.-Chim. Biol.* **1983**, *80*, 15. (c) du Mara, P.; Frascari, S.; Mariani, P.; Saturni, L.; Spada, G. P.; Tinti, M. O. *Liq. Cryst.* **1995**, *19*, 353.

(19) Charvolin, J. *Mol. Cryst. Liq. Cryst.* **1991**, *198*, 145.

(20) Borisch, K.; Diele, S.; Goering, P.; Mueller, H.; Tschierske, C. *Liq. Cryst.* **1997**, *22*, 427.

(21) (a) Donnio, B.; Bruce, D. W.; Delacroix, H.; Gulik-Krzywicki, T. *Liq. Cryst.* **1997**, *23*, 147. (b) Donnio, B.; Heinrich, B.; Gulik-Krzywicki, T.; Delacroix, H.; Guillon, D.; Bruce, D. W. *Chem. Mater.* **1997**, *9*, 2951.

(22) Fischer, S.; Fischer, H.; Diele, S.; Pelzl, G.; Jankowski, K.; Schmidt, R. R.; Vill, V. *Liq. Cryst.* **1994**, *17*, 855.

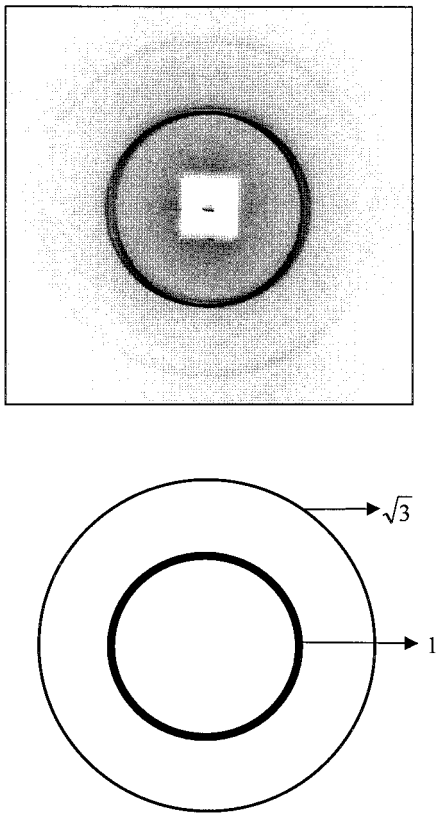


**Figure 7.** Small-angle X-ray diffraction pattern of **20-P-4** in the hexagonal columnar mesophase at 25 °C.

mass and $N_A$ is Avogadro's number. The results of this calculation are also summarized in Table 2. **15-P-4**, **17-P-4**, and **20-P-4** are calculated to have approximately seven molecules per cross section of a cylinder, which indicates the same number of molecules per cross section irrespective of the variation in the number of propylene oxide units. Similar to that in the cubic phase calculated with the inter-rod distance of 5.35 Å, the aggregation of seven rod−coil molecules in a slice can be estimated to give rise to a rectangular cross sectional aromatic core with 39 Å in width and 20 Å in length, considering that the rods are aligned axially with their preferred direction.

On the basis of the results obtained from X-ray scattering experiments and optical microscopic observations, and the above calculations, schematic representations can be constructed as shown in Figure 9. The inner core of the cylinder is composed of a discrete aromatic core with rectangular cross section while the outer by aliphatic coils which splay to fill the intercylinder matrix. This estimation is further supported by the fact that the hexagonal lattice constants observed from SAXS are in reasonable agreement with the length of rod−coil molecule with curling of the coils. The formation of the micelles with a square aromatic core has also been predicted by rod−coil theories[6a,23] and observed by experimental works,[7] and this is most probably due to a consequence of entropic penalties associated with coil stretching.

To investigate the temperature effect on the microstructure, small-angle X-ray scattering experiments have been performed with increasing temperature for **15-P-4** which exhibits a rich polymorphism (Table 1). Representative SAXS spectra measured at different temperatures and the dependence of the principal *d* spacing on temperature for rod−coil molecule **15-P-4** are presented in Figures 10 and 11, respectively. On heating as shown in Figure 11, *d* spacing shows abrupt changes at the phase transition temperatures determined by both DSC measurements and optical microscopic observations. A remarkable feature of this change in *d* spacing is the difference between values of *d* spacing for lamellar and cubic phases, which correspond to the $d_{001}$ and $d_{211}$ lattice spacings, respectively. The large reduction of *d* spacing further supports that the cubic phase exhibited by **15-P-4** consists of cylindrical networks with square cross sectional aromatic core surrounded by flexible coils as discussed earlier. In contrast, the principal *d* spacing is only slightly reduced at the phase transition from cubic phase to columnar phase, which suggests that the local structural change between these microstructures is very small.

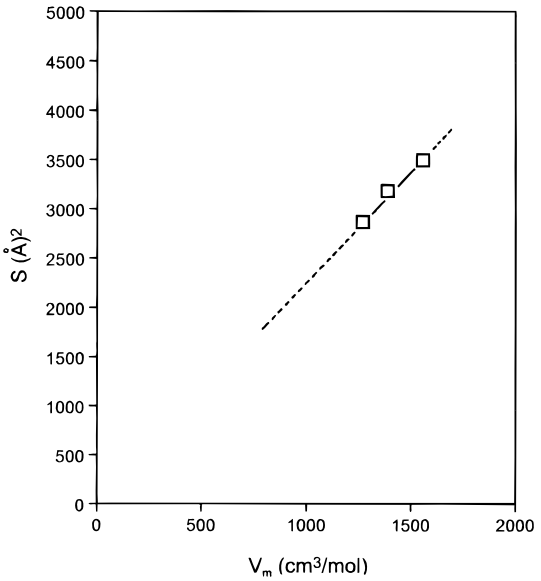


**Figure 8.** Dependence of the cross sectional area (*S*) of a cylinder on the molar volume ($V_m$) of rod−coil molecules.

According to these results, the lamellar structure seems to be most stable for the crystalline phase. With increasing temperature, the structure with large interfacial area would be required to reduce deformation free energy originated from the coil stretching in the flat interface of the lamellae. Consequently, the lamellar structure of the rod−coil molecule would break up into a new microstructure, which gives rise to a bicontinuous cubic phase with *Ia*3*d* symmetry. With further increasing temperature, the bicontinuous cubic structure may become unstable probably due to the more increased thermal motions of the coils compared to those of rods. As a result, the bicontinuous cubic structure would break up into discrete cylindrical micelles in which less confinement and stretching of coils occur, thus lowering their total free energy, leading to a hexagonal columnar phase. This is similar to the way microstructures with interfacial curvatures are formed in preference to lamellar phases in conventional diblock copolymers and lyotropic amphiphilic molecules with increasing temperature.[2,25−27]

Such molecular organizations in molecular rods are in striking contrast to what is generally accepted concerning the relationships between molecular structure and the mesomorphic phase

(23) Williams, D. R. M.; Fredrickson, G. H. *Macromolecules* **1992**, *25*, 3561.

(24) Hajduk, D. A.; Harper, P. E.; Gruner, S. M.; Honecker, C. C.; Kim, G.; Thomas, E. L.; Fetters, L. J. *Macromolecules* **1994**, *27*, 4063.

(25) (a) Schultz, M. F.; Bates, F. S.; Almdal, K.; Mortensen, K. *Phys. Rev. Lett.* **1994**, *73*, 86. (b) Koppi, K. A.; Tirrell, M.; Bates, F. S.; Almdal, K.; Mortensen, K. *J. Rheol*. **1994**, *38*, 999.

(26) (a) Alexandridis, P.; Zhou, D.; Khan, A. *Langmuir* **1996**, *12*, 2690. (b) Gido, S. P.; Wang, Z.-G. *Macromolecules* **1997**, *30*, 6771.

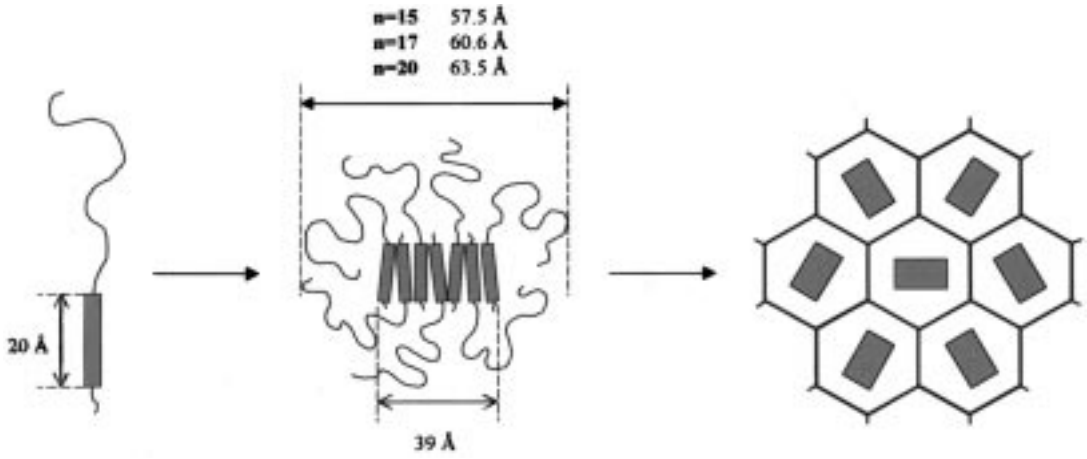


**Figure 9.** Schematic representation of the self-assembly of rod−coil molecules into a supramolecular cylinder and the subsequent formation of the hexagonal columnar liquid crystalline assembly (top view).

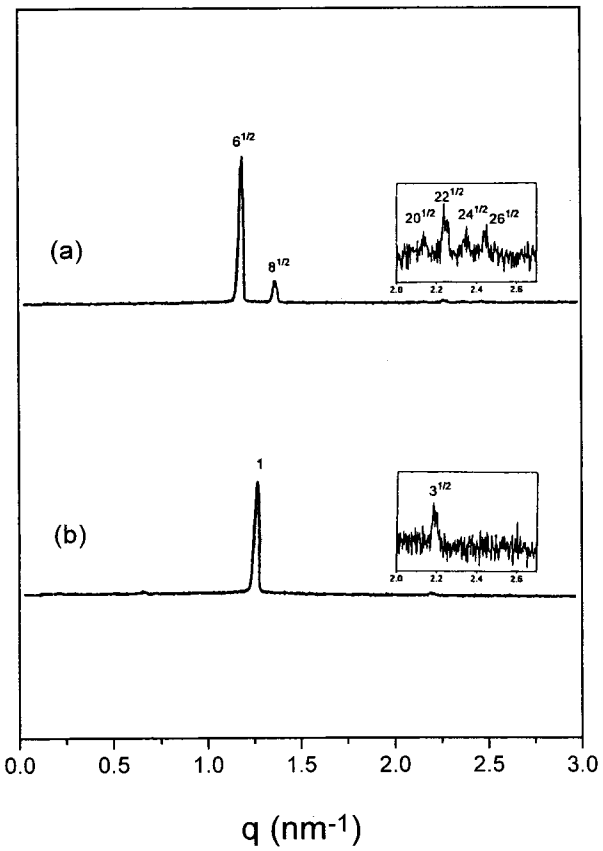


**Figure 10.** Representative SAXS spectra measured at different temperatures plotted against $q$ ($= 4\pi \sin \theta/\lambda$) in (a) the bicontinuous cubic mesophase at 26 °C and (b) the hexagonal columnar mesophase at 44 °C for **15-P-4**.

behavior of thermotropic liquid crystals. It is well established that in general the anisotropic shape of the rigid core is a main factor in determining the supramolecular structure in calamitic liquid crystalline phases.[1] In contrast, the phase behavior in the rod−coil system can be understood in terms of the fact that the main factor governing the geometry of supramolecular architecture in the liquid crystalline phase is not only the anisotropic aggregation of rod segments but also the space filling

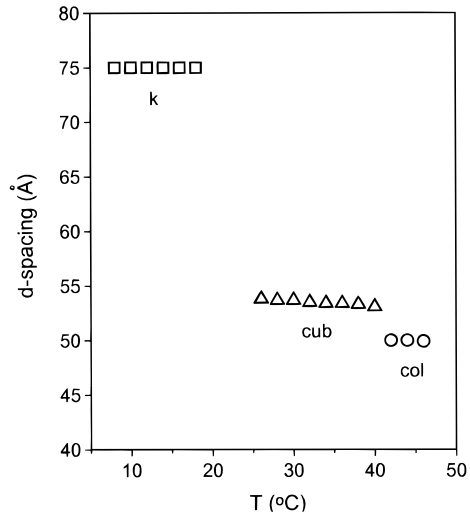


**Figure 11.** Dependence of principal $d$ spacing on temperature for **15-P-4**; □, lamellar crystalline phase ($d_{001}$); ○, bicontinuous cubic mesophase ($d_{211}$); △, hexagonal columnar mesophase ($d_{10}$).

requirements as well as entropic penalties associated with coil stretching.[4,5,23]

On the basis of the experimental results described in this study, the possible models responsible for the generation of the smectic A, bicontinuous cubic and hexagonal columnar liquid crystalline phases depending on the coil length can be presented as shown in Figure 12. The lamellar structure observed for **7-P-4** and **8-P-4** with short coil length is still the most efficient packing of amorphous coils, which is similar to that of low molar mass smectogens. As the length of the coil increases, however, space crowding of the coil segments would be large due to the increase in the number of conformational states available to the coils. Lamellar ordering of rods would confine rod−coil junctions to a flat interface with a relatively high density of grafting sites, which forces a strong stretching of the coils away from the interface and thus the system becomes unstable. Consequently, the sheetlike rod domains will break up into interwoven networks of branched cylinders with large interfacial areas in which the coils grafted onto their top and bottom surfaces fan out into a larger region of space, leading to a bicontinuous cubic phase as exhibited by **10-P-4, 12-P-4**, and **15-P-4**. This splay of the coils is reflected in the large reduction of $d$ spacing observed for rod−coil molecule **15-P-4** from 74.6 Å of the $d$ spacing in the lamellar crystalline phase to 53.9 Å of $d$ spacing in the cubic phase (Table 2 and Figure

(27) (a) Hillmeyer, M. A.; Bates, F. S.; Almdal, K.; Mortensen, K.; Ryan, A. J.; Patrick, J.; Fairclough, A. *Science* **1996**, *271*, 970. (b) Forster, S.; Khandpur, A. K.; Zhao, J.; Bates, F. S.; Hamley, I. W.; Ryan, A. J.; Bras, W. *Macromolecules* **1994**, *27*, 6922. (c) Ryan, A. J.; Fairclough, J. P. A.; Hamley, I. W.; Mai, S. M.; Booth, C. *Macromolecules* **1997**, *30*, 1723.

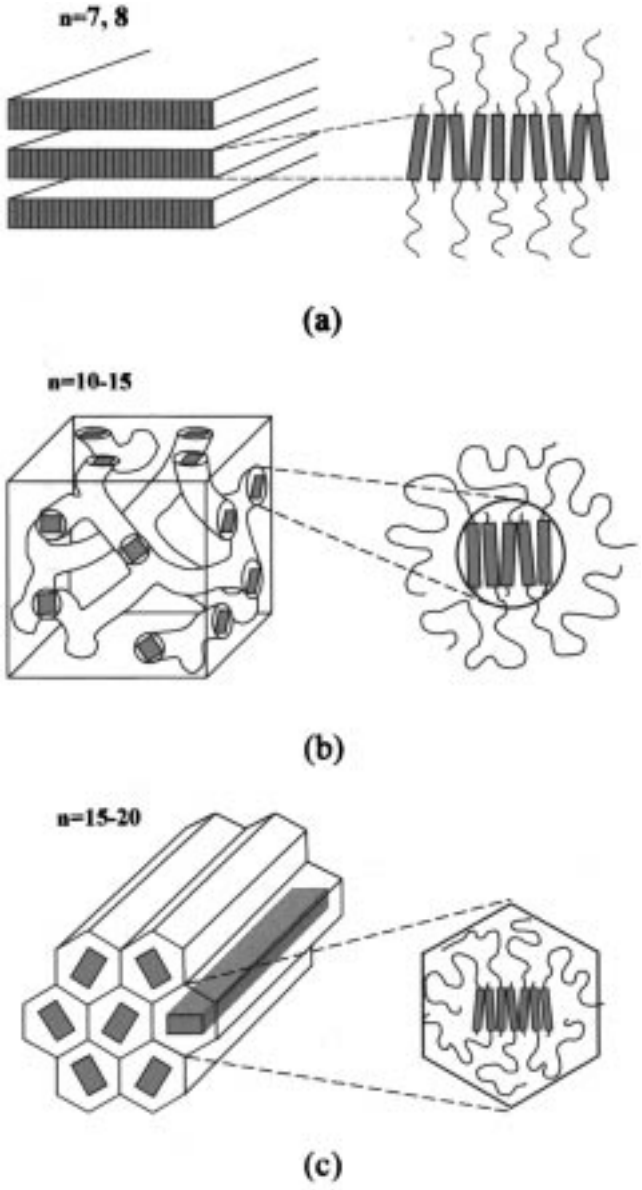


**Figure 12.** Schematic representation of the self-assemblies of the rod−coil molecules in (a) the lamellar smectic A, (b) the bicontinuous cubic, and (c) the hexagonal columnar mesophases.

11), compared to the small variation observed for rod−coil molecule **7-P-4** from 55.0 Å of layer periodicity in the crystalline phase to 45.9 Å of layer thickness in the $s_A$ phase (Table 2).

On further increasing the coil length, the bicontinuous cubic structure would break up into discrete cylindrical micelles in which less confinement and stretching of coils occurs since the micelles allow more space for coil, thus lowering their total free energy. Consequently, the bicontinuous cubic phase transforms into the cylindrical micelles which self-assemble into a hexagonal columnar mesophase as exhibited by **15-P-4, 17-P-4**, and **20-P-4**.

The phase behavior of the rod−coil molecules is similar to that in both lyotropic liquid crystals[17,26] and coil−coil diblock copolymers.[24,25,27] In comparing the rod−coil molecules and coil−coil diblock copolymers, varying the block composition or the solvent content in the latter can produce effects similar to those of both changing the temperature and changing the length of coil. Similar to coil−coil diblock system, a bicontinuous cubic phase with *Ia*3*d* symmetry is also located between lamellar and columnar phases. On the other hand, there is significant contrast between coil−coil diblock and rod−coil systems, taking into account the microphase-separated core structure for bicontinuous cubic and columnar phases. In coil−coil block copolymers, the constant density constraint on the grafted core blocks requires chain deformation. This deformation gives rise to free energy penalty favoring the micellar core with circular cross section. On the contrary, the rods consisting of a core in a rod−coil system favor the anisotropic aggregation with their long axes. As a result, this gives rise to the aromatic core with a square cross section as shown in Figures 9 and 12. The molecular organization in the rod−coil system into the cylindrical micelles is also remarkably different from that usually observed in columnar phases of disk,[15,28] half-disk,[29] and tapered molecules[30] since their molecular architecture is rodlike rather than disklike.

The results described in this paper demonstrate that systematic variation in the lengths of coils in rod−coil systems can change the supramolecular architecture from lamellar, bicontinuous cubic to cylindrical micellar phases. The main forces responsible for this change are believed to be the anisotropic orientation of rods and the resulting entropic penalties associated with coil stretching. The induction of bicontinuous cubic and hexagonal columnar phases in the molecular rod is in marked contrast to the general behavior of conventional rodlike mesogens. In this respect, our rod−coil system provides access to a large variety of experimental and theoretical investigations to fully understand the complete range of supramolecular structures formed by rod−coil diblock molecules which is essentially an unexplored area of research.

## Conclusions

The rod−coil molecules with different lengths of poly(propylene oxide) as coils were synthesized. The resulting rod−coil molecules were characterized by DSC, thermal optical microscopy, and X-ray scattering measurements. In the crystalline phase, the rod−coil molecules have been observed to organize into microphase-separated monolayer lamellar structures in which rods are fully interdigitated. Interestingly, the rod−coil molecules with 15−17 repeating units of poly(propylene oxide) have been found to exhibit rod tilt relative to the layer normal as predicted by rod−coil theories.[4−6] A dramatic mesophase change has been observed with the variation of the coil length. The rod−coil molecules **7-P-4** and **8-P-4** containing short coils self-assemble into layered smectic C and smectic A phases depending on temperature, while the rod−coil molecules with medium-length coils (**10-P-4**, **12-P-4**, and **15-P-4**) exhibit a cubic mesophase. This phase has been identified by X-ray scattering method to be a bicontinuous cubic phase with *Ia*3*d* symmetry. Further increasing the length of coil induces a hexagonal columnar mesophase as exhibited by **15-P-4**, **17-P-4**, and **20-P-4**. Calculations based on the lattice parameters and densities have shown that the organization of the rod−coil molecules into a cross sectional slice of a cylinder for the cubic and columnar phases can give rise to an aromatic core with a

(28) (a) Guillon, D.; Skoulios, A.; Piechocki, C.; Simon, J.; Weber, P. *Mol. Cryst. Liq. Cryst.* **1983**, *100*, 275. (b) Destrade, C.; Mondon, M. C.; Malthete, J. *J. Phys.* **1979**, *40-C3*, 17. (c) Gasparoux, H.; Destrade, C.; Fug, C. *Mol. Cryst. Liq. Cryst.* **1980**, *59*, 109. (d) Gasparoux, H. *Mol. Cryst. Liq. Cryst.* **1981**, *63*, 249.

(29) (a) Kleppinger, R.; Lillya, C. P.; Yang, C. *J. Am. Chem. Soc.* **1997**, *119*, 4097. (b) Kleppinger, R.; Lillya, C. P.; Yang, C. *Angew. Chem., Int. Ed. Engl.* **1995**, *34*, 1637. (c) Lee, M.; Yoo, Y.-S.; Choi, M.-G. *Bull. Kor. Chem. Soc.* **1997**, *18*, 1067.

(30) Percec, V.; Johansson, G.; Ungar, G.; Zhou, J. *J. Am. Chem. Soc.* **1996**, *118*, 9855. (b) Percec, V.; Heck, J.; Tomazos, D.; Ungar, G. *Macromol. Symp.* **1994**, *77*, 237 and references therein.

square cross section. This is a significant contrast to that in conventional cubic and columnar phases.[22,25−27] This unique behavior in the rod−coil molecules is believed to originate from the anisotropic aggregation of rod segments and consequent entropic penalties associated with coil stretching. The results described in this study demonstrate that a rich variety of self-assembled supramolecular structures can be induced in the molecular rod system through introduction of a long flexible coil.

## Experimental Section

**Materials.** 4-Hydroxy-4′-biphenylcarboxylic acid (98%), 1,3-diisopropylcarbodiimide (DIPC, 99%), toluene-*p*-sulfonyl chloride (98%), 4-(dimethylamino)pyridine (99%), poly(propylene glycol) of DPs 7, 12, and 17 (all from Aldrich), and the other conventional reagents were used as received. Poly(propylene glycol) of DPs 8, 10, 15, and 20 were synthesized according to the procedure described previously.[31] 4-(Dimethylamino)pyridinium−*p*-toluene sulfonate (DPTS) and ethyl 4-hydroxy-4′-biphenylcarboxylate were prepared as described previously.[9] Dichloromethane was dried by distillation from calcium hydride and stored over 4 Å molecular sieves. Pyridine was dried by distillation from sodium metal and stored over 4 Å molecular sieves.

**Techniques.** $^1$H NMR spectra were recorded from $CDCl_3$ solutions on a Bruker AM 250 spectrometer. The purity of the products was checked by thin-layer chromatography (TLC; Merck, silica gel 60). A Perkin-Elmer DSC-7 differential scanning calorimeter equipped with a 1020 thermal analysis controller was used to determine the thermal transitions, which were reported as the maxima and minima of their endothermic or exothermic peaks. In all cases, the heating and cooling rates were 3 °C min$^{-1}$. A Nikon Optiphot 2-pol optical polarized microscopy (magnification: ×100) equipped with a Mettler FP 82 hot-stage and a Mettler FP 90 central processor was used to observe the thermal transitions and to analyze the anisotropic texture. Microanalyses were performed with a Perkin-Elmer 240 elemental analyzer at Korea Research Institute of Chemical Technology. Molecular weight distributions were determined by gel permeation chromatography (GPC) with a Water R401 instrument equipped with Styragel HR 3, 4, and 4E columns, M7725i manual injector, column heating chamber, and 2010 Millennium data station. Measurements were made by using a UV detector with $CHCl_3$ as the solvent (1.0 mL min$^{-1}$). X-ray scattering measurements were performed in transmission mode with nickel-filtered Cu Kα radiation supplied by a Rigaku Denki generator operating at 40 kV and 40 mA and with synchrotron radiation at the 4C2 X-ray beam line with $\lambda = 0.1608$ nm at Pohang Accelerator Laboratory, Korea. To investigate structural changes on heating, the samples were held in an aluminum sample holder which was sealed with the window of 8-$\mu$m Kapton films on both sides. The samples were heated with two catridge heaters, and the temperature of the samples was monitored by a thermocouple placed close to the sample. Background scattering correction was made by subtracting the scatterings from the Kapton. The correction for the slit length smearing was applied by means of Strobl's algorithm. The density measurements were performed in an aqueous sodium chloride solution at 10 and 25 °C, respectively.

**Synthesis.** A general outline of the synthetic procedures is shown in Scheme 1.

**Oxypoly(propyleneoxy)propyl Tosylate (8−14).** Oxypoly(propyleneoxy)propyl tosylate **8** and oxypoly(propyleneoxy)propyl tosylate **9**−**14** were all synthesized using the same procedure. A representative example is described for **8**. Poly(propylene glycol) ($M_w = 425$, 28.3 g, 68.9 mmol) was dissolved in 150 mL of dry methylene chloride under nitrogen. A solution of toluene-*p*-sulfonyl chloride (45.3 g, 237.6 mmol) in 70 mL of dry methylene chloride was added under nitrogen. Then 6.27 mL of dry pyridine (77.6 mmol) was added dropwise to the mixture. The reaction mixture was stirred at room temperature under nitrogen overnight. The methylene chloride solution was washed with water, dried over anhydrous magnesium sulfate, and filtered. The solvent was removed in a rotary evaporator, and the crude product was purified by column chromatography (silica gel, ethyl acetate eluent) to yield 10.7 g (26.7%) of a colorless liquid. $^1$H NMR (250 MHz, $CDCl_3$, $\delta$, ppm): 7.80 (d, 2Ar−H, *o* to $SO_3$, $J = 8.1$ Hz), 7.31 (d, 2Ar−H, *o* to $CH_3$, $J = 8.0$ Hz), 4.65 (m, $CH_2CH(CH_3)OSO_2$ or $(CH_3)CHCH_2OSO_2$), 3.14−3.91 (m, $OCH_2CH(CH_3)$), 2.43 (s, 3H, $CH_3$phenyl), 0.99−1.28 (m, 21H, $OCH_2CH(CH_3)$).

**Oxypoly(propyleneoxy)propyl Tosylate (9)** was obtained in 10.2% yield as a colorless liquid. $^1$H NMR (250 MHz, $CDCl_3$, $\delta$, ppm): 7.80 (d, 2Ar−H, *o* to $SO_3$, $J = 7.8$ Hz), 7.29 (d, 2Ar−H, *o* to $CH_3$, $J = 7.9$ Hz), 4.62 (m, $CH_2CH(CH_3)OSO_2$ or $(CH_3)CHCH_2OSO_2$), 3.12−3.89 (m, $OCH_2CH(CH_3)$), 2.41 (s, 3H, $CH_3$phenyl), 0.97−1.25 (m, 24H, $OCH_2CH(CH_3)$).

**Oxypoly(propyleneoxy)propyl Tosylate (10)** was obtained in 12.3% yield as a colorless liquid. $^1$H NMR (250 MHz, $CDCl_3$, $\delta$, ppm): 7.80 (d, 2Ar−H, *o* to $SO_3$, $J = 7.8$ Hz), 7.29 (d, 2Ar−H, *o* to $CH_3$, $J = 7.9$ Hz), 4.62 (m, $CH_2CH(CH_3)OSO_2$ or $(CH_3)CHCH_2OSO_2$), 3.12−3.89 (m, $OCH_2CH(CH_3)$), 2.41 (s, 3H, $CH_3$phenyl), 0.97−1.25 (m, 30H, $OCH_2CH(CH_3)$).

**Oxypoly(propyleneoxy)propyl Tosylate (11)** was obtained in 27.0% yield as a colorless liquid. $^1$H NMR (250 MHz, $CDCl_3$, $\delta$, ppm): 7.77 (d, 2Ar−H, *o* to $SO_3$, $J = 8.2$ Hz), 7.31 (d, 2Ar−H, *o* to $CH_3$, $J = 7.9$ Hz), 4.63 (m, $CH_2CH(CH_3)OSO_2$ or $(CH_3)CHCH_2OSO_2$), 3.17−3.94 (m, $OCH_2CH(CH_3)$), 2.43 (s, 3H, $CH_3$phenyl), 0.95−1.20 (m, 36H, $OCH_2CH(CH_3)$).

**Oxypoly(propyleneoxy)propyl Tosylate (12)** was obtained in 17.5% yield as a colorless liquid. $^1$H NMR (250 MHz, $CDCl_3$, $\delta$, ppm): 7.82 (d, 2Ar−H, *o* to $SO_3$, $J = 8.3$ Hz), 7.34 (d, 2Ar−H, *o* to $CH_3$, $J = 8.1$ Hz), 4.67 (m, $CH_2CH(CH_3)OSO_2$ or $(CH_3)CHCH_2OSO_2$), 3.15−3.94 (m, $OCH_2CH(CH_3)$), 2.46 (s, 3H, $CH_3$phenyl), 1.02−1.32 (m, 45H, $OCH_2CH(CH_3)$).

**Oxypoly(propyleneoxy)propyl Tosylate (13)** was obtained in 26.5% yield as a colorless liquid. $^1$H NMR (250 MHz, $CDCl_3$, $\delta$, ppm): 7.78 (d, 2Ar−H, *o* to $SO_3$, $J = 8.1$ Hz), 7.29 (d, 2Ar−H, *o* to $CH_3$, $J = 8.0$ Hz), 4.63 (m, $CH_2CH(CH_3)OSO_2$ or $(CH_3)CHCH_2OSO_2$), 3.15−3.94 (m, $OCH_2CH(CH_3)$), 2.41 (s, 3H, $CH_3$phenyl), 0.99−1.26 (m, 51H, $OCH_2CH(CH_3)$).

**Oxypoly(propyleneoxy)propyl Tosylate (14)** was obtained in 15.2% yield as a colorless liquid. $^1$H NMR (250 MHz, $CDCl_3$, $\delta$, ppm): 7.78 (d, 2Ar−H, *o* to $SO_3$, $J = 8.1$ Hz), 7.29 (d, 2Ar−H, *o* to $CH_3$, $J = 8.0$ Hz), 4.63 (m, $CH_2CH(CH_3)OSO_2$ or $(CH_3)CHCH_2OSO_2$), 3.14−3.90 (m, $OCH_2CH(CH_3)$), 2.42 (s, 3H, $CH_3$phenyl), 0.98−1.27 (m, 60H, $OCH_2CH(CH_3)$).

**4-[Oxypoly(propyleneoxy)propyloxy]-4′-biphenylcarboxylic Acid (15−21).** 4-[Oxypoly(propyleneoxy)propyloxy]-4′-biphenylcarboxylic acid (**15**) and 4′-[Oxy poly(propyleneoxy)propyloxy]-4-biphenyl carboxylic acids **16**−**21** were all synthesized using the same procedure. A representative example is described for **15**. Oxypoly(propyleneoxy)-propyl tosylate (**8**) (6.5 g, 11.3 mmol), ethyl 4-hydroxy-4′-biphenylcarboxylate (8.2 g, 33.9 mmol), and excess $K_2CO_3$ were dissolved in 250 mL of ethanol. The mixture was heated at reflux for 24 h and then cooled to room temperature and excess KOH was added. The mixture solution was stirred at room temperature for 3 h. The resulting solution was poured into water and extracted with methylene chloride. The methylene chloride solution was washed with water, dried over anhydrous magnesium sulfate, and filtered. After the solvent was removed in a rotary evaporator, 4.2 g (60.2%) of a colorless liquid was yielded. $^1$H NMR (250 MHz, $CDCl_3$, $\delta$, ppm): 8.13 (d, 2Ar−H, *o* to COOH, $J = 8.4$ Hz), 7.64 (d, 2Ar−H, *m* to COOH, $J = 8.4$ Hz), 7.55 (d, 2Ar−H, *m* to $CH(CH_3)O$, $J = 8.7$ Hz), 7.02 (d, 2Ar−H, *o* to $CH(CH_3)O$, $J = 8.5$ Hz), 4.57 (m, $CH_2CH(CH_3)$Ophenyl or $(CH_3)CHCH_2$Ophenyl), 3.15−4.00 (m, $OCH_2CH(CH_3)$, 0.85−1.37 (m, 21H, $OCH_2CH(CH_3)$). Anal. Calcd for $C_{34}H_{52}O_{10}$: C, 65.78; H, 8.44. Found: C, 65.88; H, 8.52.

**4-[Oxypoly(propyleneoxy)propyloxy]-4′-biphenylcarboxylic Acid (16)** was obtained in 63.4% yield as a colorless liquid. $^1$H NMR (250 MHz, $CDCl_3$, $\delta$, ppm): 8.13 (d, 2Ar−H, *o* to COOH, $J = 8.1$ Hz), 7.63 (d, 2Ar−H, *m* to COOH, $J = 8.2$ Hz), 7.55 (d, 2Ar−H, *m* to $CH(CH_3)O$, $J = 8.2$ Hz), 7.01 (d, 2Ar−H, *o* to $CH(CH_3)O$, $J = 8.2$ Hz), 4.57 (m, $CH_2CH(CH_3)$Ophenyl or $(CH_3)CHCH_2$Ophenyl), 3.15−

(31) Lauter, U.; Meyer, W. H.; Wegner, G. *Macromolecules* **1997**, *30*, 2092.

4.02 (m, OC$H_2$C$H$(CH$_3$), 0.85−1.37 (m, 24H, OCH$_2$CH(C$H_3$)). Anal. Calcd for $C_{37}H_{58}O_{11}$: C, 65.46; H, 8.61. Found: C, 65.51; H, 8.96.

**4-[Oxypoly(propyleneoxy)propyloxy]-4′-biphenylcarboxylic Acid (17)** was obtained in 60.4% yield as a colorless liquid. $^1$H NMR (250 MHz, CDCl$_3$, $\delta$, ppm): 8.13 (d, 2Ar−H, *o* to COOH, $J$ = 7.1 Hz), 7.64 (d, 2Ar−H, *m* to COOH, $J$ = 7.2 Hz), 7.55 (d, 2Ar−H, *m* to CH(CH$_3$)O, $J$ = 7.4 Hz), 7.01 (d, 2Ar−H, *o* to CH(CH$_3$)O, $J$ = 8.2 Hz), 4.57 (m, CH$_2$C$H$(CH$_3$)Ophenyl or (CH$_3$)CHC$H_2$Ophenyl), 3.15−4.02 (m, OC$H_2$C$H$(CH$_3$), 0.85−1.37 (m, 30H, OCH$_2$CH(C$H_3$)). Anal. Calcd for $C_{43}H_{70}O_{13}$: C, 64.96; H, 8.87. Found: C, 64.51; H, 8.76.

**4-[Oxypoly(propyleneoxy)propyloxy]-4′-biphenylcarboxylic Acid (18)** was obtained in 64.0% yield as a colorless liquid. $^1$H NMR (250 MHz, CDCl$_3$, $\delta$, ppm): 8.12 (d, 2Ar−H, *o* to COOH, $J$ = 8.5 Hz), 7.58 (d, 2Ar−H, *m* to COOH, $J$ = 8.5 Hz), 7.52 (d, 2Ar−H, *m* to CH(CH$_3$)O, $J$ = 8.5 Hz), 6.99 (d, 2Ar−H, *o* to CH(CH$_3$)O, $J$ = 8.5 Hz), 4.56 (m, CH$_2$C$H$(CH$_3$)Ophenyl or (CH$_3$)CHC$H_2$Ophenyl), 3.15−4.05 (m, OC$H_2$C$H$(CH$_3$), 0.85−1.37 (m, 36H, OCH$_2$CH(C$H_3$)). Anal. Calcd for $C_{49}H_{82}O_{15}$: C, 64.59; H, 9.07. Found: C, 64.48; H, 9.17.

**4-[Oxypoly(propyleneoxy)propyloxy]-4′-biphenylcarboxylic Acid (19)** was obtained in 63.8% yield as a colorless liquid. $^1$H NMR (250 MHz, CDCl$_3$, $\delta$, ppm): 8.12 (d, 2Ar−H, *o* to COOH, $J$ = 8.5 Hz), 7.57 (d, 2Ar−H, *m* to COOH, $J$ = 8.5 Hz), 7.53 (d, 2Ar−H, *m* to CH(CH$_3$)O, $J$ = 8.5 Hz), 7.03 (d, 2Ar−H, *o* to CH(CH$_3$)O, $J$ = 8.5 Hz), 4.59 (m, CH$_2$C$H$(CH$_3$)Ophenyl or (CH$_3$)CHC$H_2$Ophenyl), 3.14−4.03 (m, OC$H_2$C$H$(CH$_3$), 0.84−1.37 (m, 45H, OCH$_2$CH(C$H_3$)). Anal. Calcd for $C_{58}H_{100}O_{18}$: C, 64.18; H, 9.29. Found: C, 64.19; H, 9.38.

**4-[Oxypoly(propyleneoxy)propyloxy]-4′-biphenylcarboxylic Acid (20)** was obtained in 58.7% yield as a colorless liquid. $^1$H NMR (250 MHz, CDCl$_3$, $\delta$, ppm): 8.12 (d, 2Ar−H, *o* to COOH, $J$ = 8.0 Hz), 7.63 (d, 2Ar−H, *m* to COOH, $J$ = 8.1 Hz), 7.55 (d, 2Ar−H, *m* to CH(CH$_3$)O, $J$ = 8.4 Hz), 7.02 (d, 2Ar−H, *o* to CH(CH$_3$)O, $J$ = 8.2 Hz), 4.56 (m, CH$_2$C$H$(CH$_3$)Ophenyl or (CH$_3$)CHC$H_2$Ophenyl), 3.14−3.93 (m, OC$H_2$C$H$(CH$_3$), 0.84−1.36 (m, 51H, OCH$_2$CH(C$H_3$)). Anal. Calcd for $C_{64}H_{112}O_{20}$: C, 63.97; H, 9.40. Found: C, 64.31; H, 9.01.

**4-[Oxypoly(propyleneoxy)propyloxy]-4′-biphenylcarboxylic Acid (21)** was obtained in 59.2% yield as a colorless liquid. $^1$H NMR (250 MHz, CDCl$_3$, $\delta$, ppm): 8.12 (d, 2Ar−H, *o* to COOH, $J$ = 8.3 Hz), 7.63 (d, 2Ar−H, *m* to COOH, $J$ = 8.3 Hz), 7.55 (d, 2Ar−H, *m* to CH(CH$_3$)O, $J$ = 8.7 Hz), 7.02 (d, 2Ar−H, *o* to CH(CH$_3$)O, $J$ = 7.6 Hz), 4.57 (m, CH$_2$C$H$(CH$_3$)Ophenyl or (CH$_3$)CHC$H_2$Ophenyl), 3.16−3.93 (m, OC$H_2$C$H$(CH$_3$), 0.84−1.37 (m, 60H, OCH$_2$CH(C$H_3$)). Anal. Calcd for $C_{73}H_{130}O_{23}$: C, 63.73; H, 9.52. Found: C, 63.87; H, 9.23.

**Ethyl 4-[4-[Oxypoly(propyleneoxy)propyloxy]-4′-biphenylcarboxyloxy]-4′-biphenylcarboxylate (*n*-P-4).** Ethyl 4-[4-[oxypoly(propyleneoxy)propyloxy]-4′-biphenylcarboxyloxy]-4′-biphenylcarboxylate **7-P-4** and ethyl 4-[4-[oxypoly(propyleneoxy)propyloxy]-4′-biphenylcarboxyloxy]-4′-biphenylcarboxylates **8-P-4, 10-P-4, 12-P-4, 15-P-4, 17-P-4**, and **20-P-4** were all synthesized using the same procedure. A representative example is described for **7-P-4**. 4-[Oxypoly(propyleneoxy)propyloxy]-4′-biphenylcarboxylic acid (**15**) (5.7 g, 9.1 mmol), ethyl 4-hydroxy-4′-biphenylcarboxylate (6.6 g, 27.2 mmol), and 4-(dimethylamino)pyridinium−*p*-toluene sulfonate (DPTS, 0.63 g, 2.1 mmol) were dissolved in 100 mL of dry methylene chloride under nitrogen. And then 1,3-diisopropylcarbodiimide (DIPC, 1.42 mL, 9.1 mmol) was added dropwise to the mixture. The mixture was stirred at room temperature under nitrogen overnight. The resulting solution was poured into water and extracted with methylene chloride. The methylene chloride solution was washed with water, dried over anhydrous magnesium sulfate, and filtered. The solvent was removed in a rotary evaporator, and the crude product was purified by column chromatography (silica gel, ethyl acetate) to yield 3.7 g (yield: 47.8%) of a white solid. $^1$H NMR (250 MHz, CDCl$_3$, $\delta$, ppm): 8.26 (d, 2Ar−H, *o* to COOphenyl, $J$ = 8.2 Hz), 8.13 (d, 2Ar−H, *o* to COOCH$_2$, $J$ = 8.2 Hz), 7.65−7.72 (m, 6Ar−H, *m* to COOphenyl, *m* to biphenylcarboxylate and *m* to COOCH$_2$), 7.60 (d, 2Ar−H, *m* to CH(CH$_3$)O, $J$ = 8.6 Hz), 7.34 (d, 2Ar−H, *o* to biphenylcarboxylate, $J$ = 8.4 Hz), 7.04 (d, 2Ar−H, *o* to CH(CH$_3$)O, $J$ = 8.3 Hz), 4.58 (m, CH$_2$C$H$(CH$_3$)Ophenyl or (CH$_3$)CHC$H_2$Ophenyl), 4.41 (q, 2H, OC$H_2$CH$_3$, $J$ = 7.1 Hz), 3.18−3.92 (m, OC$H_2$C$H$(CH$_3$)), 1.35−1.45 (m, 6H, CH$_2$C$H_3$ and CH(C$H_3$)Ophenyl), 0.90−1.30 (m, 18H, OCH$_2$CH(C$H_3$)). $^{13}$C NMR (62.5 MHz, CDCl$_3$, $\delta$, ppm): 166.4, 165.0, 158.6, 158.5, 151.1, 146.0, 144.6, 137.7, 132.1, 130.7, 130.1, 129.3, 128.3, 127.3, 126.9, 126.6, 122.2, 116.4, 72.3−76.0, 67.2, 65.5, 61.0, 16.9−18.4, 14.3. Anal. Calcd for $C_{49}H_{64}O_{12}$: C, 69.65; H, 7.63. Found: C, 69.69; H, 7.30.

**Ethyl 4-[4-[Oxypoly(propyleneoxy)propyloxy]-4′-biphenylcarboxyloxy]-4′-biphenylcarboxylate (8-P-4)** was obtained in 43.5% yield as a white solid. $^1$H NMR (250 MHz, CDCl$_3$, $\delta$, ppm): 8.25 (d, 2Ar−H, *o* to COOphenyl, $J$ = 8.4 Hz), 8.12 (d, 2Ar−H, *o* to COOCH$_2$, $J$ = 8.3 Hz), 7.65−7.72 (m, 6Ar−H, *m* to COOphenyl, *m* to biphenylcarboxylate and *m* to COOCH$_2$), 7.59 (d, 2Ar−H, *m* to CH(CH$_3$)O, $J$ = 8.7 Hz), 7.33 (d, 2Ar−H, *o* to biphenylcarboxylate, $J$ = 8.6 Hz), 7.04 (d, 2Ar−H, *o* to CH(CH$_3$)O, $J$ = 8.4 Hz), 4.58 (m, CH$_2$C$H$(CH$_3$)Ophenyl or (CH$_3$)CHC$H_2$Ophenyl), 4.41 (q, 2H, OC$H_2$CH$_3$, $J$ = 7.1 Hz), 3.14−3.94 (m, OC$H_2$C$H$(CH$_3$)), 1.34−1.45 (m, 6H, CH$_2$C$H_3$ and CH(C$H_3$)Ophenyl), 0.90−1.30 (m, 21H, OCH$_2$CH(C$H_3$)). $^{13}$C NMR (62.5 MHz, CDCl$_3$, $\delta$, ppm): 166.4, 165.0, 158.5, 158.5, 151.1, 146.0, 144.6, 137.7, 132.1, 130.7, 130.1, 129.3, 128.3, 127.3, 126.9, 126.6, 122.2, 116.4, 73.3−75.7, 67.2, 65.5, 60.9, 16.9−18.4, 14.3. Anal. Calcd for $C_{52}H_{70}O_{13}$: C, 69.16; H, 7.81. Found: C, 69.52; H, 7.76.

**Ethyl 4-[4-[Oxypoly(propyleneoxy)propyloxy]-4′-biphenylcarboxyloxy]-4′-biphenylcarboxylate (10-P-4)** was obtained in 44.6% yield as a white solid. $^1$H NMR (250 MHz, CDCl$_3$, $\delta$, ppm): 8.26 (d, 2Ar−H, *o* to COOphenyl, $J$ = 8.4 Hz), 8.12 (d, 2Ar−H, *o* to COOCH$_2$, $J$ = 8.4 Hz), 7.65−7.72 (m, 6Ar−H, *m* to COOphenyl, *m* to biphenylcarboxylate and *m* to COOCH$_2$), 7.59 (d, 2Ar−H, *m* to CH(CH$_3$)O, $J$ = 8.7 Hz), 7.34 (d, 2Ar−H, *o* to biphenylcarboxylate, $J$ = 8.6 Hz), 7.04 (d, 2Ar−H, *o* to CH(CH$_3$)O, $J$ = 8.4 Hz), 4.58 (m, CH$_2$C$H$(CH$_3$)Ophenyl or (CH$_3$)CHC$H_2$Ophenyl), 4.41 (q, 2H, OC$H_2$CH$_3$, $J$ = 7.1 Hz), 3.18−3.95 (m, OC$H_2$C$H$(CH$_3$)), 1.34−1.45 (m, 6H, CH$_2$C$H_3$ and CH(C$H_3$)Ophenyl), 0.90−1.31 (m, 27H, OCH$_2$CH(C$H_3$)). $^{13}$C NMR (62.5 MHz, CDCl$_3$, $\delta$, ppm): 166.4, 165.0, 158.5, 158.5, 151.1, 146.0, 144.6, 137.7, 132.1, 130.7, 130.1, 129.3, 128.3, 127.3, 126.9, 126.6, 122.2, 116.4, 72.3−76.0, 67.2, 65.5, 61.0, 16.9−18.4, 14.3. Anal. Calcd for $C_{58}H_{82}O_{15}$: C, 68.35; H, 8.11. Found: C, 68.28; H, 8.45.

**Ethyl 4-[4-[Oxypoly(propyleneoxy)propyloxy]-4′-biphenylcarboxyloxy]-4′-biphenylcarboxylate (12-P-4)** was obtained in 50.0% yield as a white solid. $^1$H NMR (250 MHz, CDCl$_3$, $\delta$, ppm): 8.24 (d, 2Ar−H, *o* to COOphenyl, $J$ = 7.8 Hz), 8.12 (d, 2Ar−H, *o* to COOCH$_2$, $J$ = 7.7 Hz), 7.65−7.71 (m, 6Ar−H, *m* to COOphenyl, *m* to biphenylcarboxylate and *m* to COOCH$_2$), 7.59 (d, 2Ar−H, *m* to CH(CH$_3$)O, $J$ = 8.5 Hz), 7.35 (d, 2Ar−H, *o* to biphenylcarboxylate, $J$ = 8.5 Hz), 7.04 (d, 2Ar−H, *o* to CH(CH$_3$)O, $J$ = 8.6 Hz), 4.58 (m, CH$_2$C$H$(CH$_3$)Ophenyl or (CH$_3$)CHC$H_2$Ophenyl), 4.41 (q, 2H, OC$H_2$CH$_3$, $J$ = 7.1 Hz), 3.15−3.91 (m, OC$H_2$C$H$(CH$_3$)), 1.34−1.45 (m, 6H, CH$_2$C$H_3$ and CH(C$H_3$)Ophenyl), 0.90−1.30 (m, 27H, OCH$_2$CH(C$H_3$)). $^{13}$C NMR (62.5 MHz, CDCl$_3$, $\delta$, ppm): 166.4, 165.0, 158.6, 158.5, 151.1, 146.1, 144.7, 137.8, 132.1, 130.7, 130.1, 129.3, 128.4, 127.3, 127.0, 126.6, 122.2, 116.4, 72.9−75.5, 67.2, 65.6, 61.0, 16.9−18.4, 14.3. Anal. Calcd for $C_{64}H_{94}O_{17}$: C, 67.70; H, 8.34. Found: C, 67.72; H, 8.48.

**Ethyl 4-[4-[Oxypoly(propyleneoxy)propyloxy]-4′-biphenylcarboxyloxy]-4′-biphenylcarboxylate (15-P-4)** was obtained in 48.2% yield as a white solid. $^1$H NMR (250 MHz, CDCl$_3$, $\delta$, ppm): 8.24 (d, 2Ar−H, *o* to COOphenyl, $J$ = 7.8 Hz), 8.12 (d, 2Ar−H, *o* to COOCH$_2$, $J$ = 7.7 Hz), 7.65−7.71 (m, 6Ar−H, *m* to COOphenyl, *m* to biphenylcarboxylate and *m* to COOCH$_2$), 7.59 (d, 2Ar−H, *m* to CH(CH$_3$)O, $J$ = 8.5 Hz), 7.31 (d, 2Ar−H, *o* to biphenylcarboxylate, $J$ = 8.5 Hz), 7.04 (d, 2Ar−H, *o* to CH(CH$_3$)O, $J$ = 8.6 Hz), 4.58 (m, CH$_2$C$H$(CH$_3$)Ophenyl or (CH$_3$)CHC$H_2$Ophenyl), 4.41 (q, 2H, OC$H_2$CH$_3$, $J$ = 7.1 Hz), 3.15−3.92 (m, OC$H_2$C$H$(CH$_3$)), 1.34−1.45 (m, 6H, CH$_2$C$H_3$ and CH(C$H_3$)Ophenyl), 0.85−1.34 (m, 42H, OCH$_2$CH(C$H_3$)). $^{13}$C NMR (62.5 MHz, CDCl$_3$, $\delta$, ppm): 166.4, 165.0, 158.6, 158.5, 151.0, 146.0, 144.6, 137.7, 132.0, 130.7, 130.1, 129.3, 128.3, 127.3, 126.9, 126.6, 122.2, 116.3, 72.6−76.0, 67.1, 65.5, 60.9, 16.9−18.4, 14.3. Anal. Calcd for $C_{73}H_{112}O_{20}$: C, 66.95; H, 8.62. Found: C, 67.24; H, 8.71.

**Ethyl 4-[4-[Oxypoly(propyleneoxy)propyloxy]-4′-biphenylcarboxyloxy]-4′-biphenylcarboxylate (17-P-4)** was obtained in 43.3% yield as a white solid. $^1$H NMR (250 MHz, CDCl$_3$, $\delta$, ppm): 8.25 (d, 2Ar−H, *o* to COOphenyl, $J$ = 8.3 Hz), 8.11 (d, 2Ar−H, *o* to COOCH$_2$, $J$ = 8.3 Hz), 7.64−7.71 (m, 6Ar−H, *m* to COOphenyl, *m* to

biphenylcarboxylate and *m* to $COOCH_2$), 7.58 (d, 2Ar−H, *m* to CH-$(CH_3)$O, $J$ = 8.7 Hz), 7.33 (d, 2Ar−H, *o* to biphenylcarboxylate, $J$ = 8.6 Hz), 7.03 (d, 2Ar−H, *o* to $CH(CH_3)O$, $J$ = 8.2 Hz), 4.58 (m, $CH_2CH(CH_3)$Ophenyl or $(CH_3)CHCH_2$Ophenyl), 4.40 (q, 2H, $OCH_2$-$CH_3$, $J$ = 7.1 Hz), 3.14−3.91 (m, $OCH_2CH(CH_3)$), 1.35−1.44 (m, 6H, $CH_2CH_3$ and $CH(CH_3)$Ophenyl), 0.85−1.34 (m, 48H, $OCH_2CH(CH_3)$). $^{13}$C NMR (62.5 MHz, $CDCl_3$, $\delta$, ppm): 166.4, 165.0, 158.6, 158.5, 151.1, 146.0, 144.6, 137.7, 132.1, 130.7, 130.1, 129.3, 128.4, 127.3, 126.9, 126.6, 122.2, 116.4, 72.9−75.5, 67.2, 65.5, 60.9, 16.9−18.4, 14.3. Anal. Calcd for $C_{79}H_{124}O_{22}$: C, 66.55; H, 8.77. Found: C, 66.52; H, 8.55.

**Ethyl 4-[4-[Oxypoly(propyleneoxy)propyloxy]-4′-biphenylcarboxyloxy]-4′-biphenylcarboxylate (20-P-4)** was obtained in 45.3% yield as a white solid. $^1$H NMR (250 MHz, $CDCl_3$, $\delta$, ppm): 8.26 (d, 2Ar−H, *o* to COOphenyl, $J$ = 8.4 Hz), 8.13 (d, 2Ar−H, *o* to $COOCH_2$, $J$ = 8.3 Hz), 7.65−7.72 (m, 6Ar−H, *m* to COOphenyl, *m* to biphenylcarboxylate, and *m* to $COOCH_2$), 7.60 (d, 2Ar−H, *m* to CH-$(CH_3)$O, $J$ = 8.7 Hz), 7.33 (d, 2Ar−H, *o* to biphenylcarboxylate, $J$ = 8.6 Hz), 7.04 (d, 2Ar−H, *o* to $CH(CH_3)O$, $J$ = 8.6 Hz), 4.58 (m, $CH_2CH(CH_3)$Ophenyl or $(CH_3)CHCH_2$Ophenyl), 4.41 (q, 2H, $OCH_2$-$CH_3$, $J$ = 7.1 Hz), 3.15−3.91 (m, $OCH_2CH(CH_3)$), 1.35−1.44 (m, 6H, $CH_2CH_3$ and $CH(CH_3)$Ophenyl), 0.85−1.34 (m, 66H, $OCH_2CH(CH_3)$). $^{13}$C NMR (62.5 MHz, $CDCl_3$, $\delta$, ppm): 166.5, 165.1, 158.6, 158.5, 151.1, 146.1, 144.7, 137.8, 132.1, 130.8, 130.1, 129.3, 128.4, 127.3, 127.0, 126.6, 122.3, 116.4, 72.9−76.5, 67.2, 65.5, 61.0, 17.2−18.1, 14.4. Anal. Calcd for $C_{88}H_{142}O_{25}$: C, 66.06; H, 8.95. Found: C, 65.69; H, 8.93.

**Acknowledgment.** Financial support of this work by the Ministry of Education, Republic of Korea (BSRI-97-3422), the Korea Science and Engineering Foundation (971-0301-004-2), and the Synchrotron Radiation Source at Pohang, Korea (for the beamtime and technical assistance), is gratefully acknowledged. W.-C.Z. acknowledges the Korea Ministry of Education for research fund.

**Supporting Information Available:** Representative optical polarized micrographs for **7-P-4** and **15-P-4** (1 page, print/PDF). See any current masthead page for ordering information and Web access instructions.

JA980654W